Synthesis of C^0 Path Generating Contact-Aided Compliant Mechanisms using the Material Mask Overlay Method

Prabhat Kumar[a], Roger A. Sauer[b], and Anupam Saxena[*a]

[a]Mechanical Engineering , Indian Institute of Technology Kanpur, 208016, India , kprabhat@iitk.ac.in
[b]Mechanical Engineering , AICES, RWTH Aachen University, Templergraben 55, 52056 Aachen, Germany, sauer@aices.rwth-aachen.de
[a]Mechanical Engineering , Indian Institute of Technology Kanpur, 208016, India , anupams@iitk.ac.in

Published[1] in *Journal of Mechanical Engineering* doi: 10.1115/1.4033393
Submitted on 11. May 2015, Revised on 08. April 2016, Accepted on 27. April 2016

Abstract Contact-Aided Compliant Mechanisms (CCMs) are synthesized via the Material Mask Overlay Strategy (MMOS) to trace desired non-smooth paths. MMOS employs hexagonal cells to discretize the design region and engages negative circular masks to designate material states. To synthesize CCMs, the modified MMOS presented herein involves systematic mutation of five mask parameters through a hill climber search to evolve not only the continuum topology, but also, to position the rigid, interacting surfaces within some masks. To facilitate analysis with contact, boundary smoothing is performed by shifting boundary nodes of the evolving continuum. Various geometric singularities are subdued via hexagonal cells and the V-notches at the continuum boundaries are alleviated. Numerous hexagonal cells get morphed into concave sub-regions as a consequence. Large deformation finite element formulation with Mean Value Coordinates (MVC) based shape functions is used to cater to the generic hexagonal shapes. Contact analysis is accomplished via the Newton-Raphson iteration with load incrementing in conjunction with the augmented Lagrange multiplier method and active set constraints. An objective function based on Fourier Shape Descriptors is minimized subject to suitable design constraints. Two examples of path generating CCMs are presented, their performance compared with a commercial software, and fabricated to establish the efficacy of the proposed synthesis method.
Keywords: MMOS; Contact-aided compliant mechanisms; Hexagonal tessellation; Boundary smoothing; Fourier Shape Descriptors.

1 Introduction

1.1 Compliant Mechanisms

Compliant mechanisms (CMs) transfer input loads to a desired output by virtue of some or all of their deforming members. Two well-established methods e.g., the Pseudo Rigid Body Model

*Corresponding author, email: anupams@iitk.ac.in
[1]This pdf is the personal version of an article whose final publication is available at http://asmedigitalcollection.asme.org

and the continuum optimization approaches, exist to synthesize CMs. Among the topology optimization approaches, the Homogenization method by Kikuchi and Bendsøe [1] aimed at determining the optimal size of an elliptic void within a solid cell. An array of such cells comprised the stiffest possible structure under a resource constraint. Ananthasuresh [2] extended the Homogenization approach to synthesize compliant mechanisms systematically. Ananthasuresh et al. [3] maximized the desired output displacement in addition to maximizing stiffness of the mechanism. Frecker et al. [4] and Nishiwaki et al. [5] used ratio of the two objectives and reported improvement in convergence. Using the SIMP (Solid Isotropic Method with Penalization) method [6–8], Sigmund [9] proposed to maximize the mechanical advantage with suitable constraints on input displacements and volume. In SIMP, cell density (ρ_i) is considered a design variable. $\rho_i = \epsilon > 0$ models void cells [2] while $\rho_i = 1$ models cells with the desired material. The elastic modulus of a cell is modeled as $E_i = E_0\rho_i^n$, where n (≥ 3) is a penalty parameter to help accelerate the optimization algorithm to converge towards a binary solution. E_0 is the modulus of the desired material. To design compliant mechanisms, other material models similar to SIMP were based on the normal distribution (the PEAK model [10]) and logistic functions (the SIGMOID model [11]).

Most aforementioned methods employed rectangular shaped cells to analyze the evolving continuum via the finite element analysis. These discretization schemes suffer from geometric singularities like the checkerboard patterns, point flexures and islanding [12] to circumvent which, additional suppression, filtering or penalty based methods are required [13–19]. Rahamatalla and Swan [12] proposed a two stage optimization formulation by introducing artificial springs, one at the input location and an other at the output position. They suggested increasing the stiffness of springs attached to the output port to obtain compliant mechanisms free from point flexures.

Numerous similar approaches in topology optimization used discrete (truss, and/or frame elements) or continuum (rectangular, hexagonal or polygonal cells) parameterization and optimized various measures of flexibility and stiffness (generalized in Reference [20]) to synthesize monolithic compliant mechanisms under the small deformation assumption.

Path generating compliant mechanisms undergo large deflections to trace a specified path. Saxena and Ananthasuresh [21] and Pedersen et al. [22] considered geometric nonlinearity in their synthesis methods. Objectives based on least square errors [21–23] were employed to minimize the discrepancy in the specified and actual paths. The least square objective fails to compare the shape, size and orientation of the two paths individually. Ullah and Kota [24] employed Fourier Shape Descriptors [25] to exercise individual control over the shape, size and orientation of paths. Rai et al. [26, 27] demonstrated that large, nonlinear and nonsmooth paths can be traced by an assemblage of deformable curved and rigid linear members to synthesize path generating fully and partially compliant mechanisms respectively. The latter, even though capable of tracing a desired non-smooth path, required significant effort and care when assembling different components.

1.2 Contact-Aided Compliant Mechanisms

The notion of contact based deformation was first proposed and exploited by Mankame and Ananthasuresh [28, 29] to achieve non-smooth paths via monolithic (fully) compliant mechanisms. A contact-aided compliant mechanism (CCM), by constitution, is a monolithic mechanism but behaves like a partially compliant mechanism at instance(s) in its deformation history wherein members come into contact thereby introducing pseudo hinges/sliding pairs. That is, prior to contact, CCMs behave like fully compliant mechanisms while post contact, they behave like partially compliant mechanisms. Need for assembly is eliminated since a CCM is a

[2] A small positive ϵ is chosen to circumvent singularity in the stiffness matrix during the finite element analysis.

jointless continuum and friction/wear and/or need for lubrication is significantly reduced if the number of contact sites are much less than say, the number of hinges in a partially compliant mechanism [27]. Moreover, in the latter, friction always exists at rigid-body joints while in a contact-aided compliant mechanism, friction comes into play only when members interact physically. Internal contact(s), as in a CCM, seem essential to impart sudden changes in the continuum response, a phenomenon that can be utilized in say, tracing a path that is C^0 continuous, and attaining interesting deformation characteristics like negative stiffness and static balancing. For topology synthesis of CCMs, linear [23, 28] and curved frame elements [26, 30] have been employed previously for design parameterization and geometrically nonlinear finite element analysis. Intermittent but prespecified contact surfaces were used in Reference [28]. Reddy et al. [30] synthesized monolithic, path generating CCMs by modeling the design region with discrete curved members. Contact surfaces were not prespecified, rather determined systematically.

2 Motivation and Organization

We demonstrate topology synthesis of C^0 path generating contact-aided compliant mechanisms[3] via a novel approach that entails continuous discretization of the design region. We employ hexagonal cells for domain representation and negative circular masks to not only help identify the continuum topology, but also, to suspend rigid contact surfaces in the neighborhood so that the continuum can interact physically with such surfaces.

The paper is organized as follows: In section 3, the Material Mask Overlay Method is discussed briefly followed by its modified version to synthesize CCMs. Sections 4 and 5 outline boundary smoothing and large deformation finite element analysis with contact. Section 6 describes the path generating objective based on Fourier Shape Descriptors with suitable modification to control the resource volume. The hill climber search algorithm is also discussed. Synthesis results and fabricated prototypes are analyzed in section 7. Finally, section 8 outlines discussion and conclusions.

3 Material Masks Overlay Strategy (MMOS)

The previously proposed Material Mask Overlay Method (MMOS) [18, 31] uses hexagonal cells (Ω_{H}) for domain (Ω) discretization and engages negative circular masks (Ω_{M}) to designate the material state $\rho(\Omega_{\mathrm{H}})$ to each cell within the domain. Through hexagonal tessellation, *edge-connectivity* is ensured throughout thereby guaranteeing finite stiffness everywhere within the design region. Each Ω_{M} is associated with three variables (x_i, y_i, r_i), where (x_i, y_i) are center coordinates of the mask and r_i is its radius. All cells with centroids inside any mask are modeled *void*. The continuum is thus defined by the set of remnant cells that are not exposed to any mask. Mathematically, the material state of a cell is described as

$$\rho(\Omega_{\mathrm{H}}) = \begin{cases} 0, & \text{if } \Omega_{\mathrm{H}}^{\mathrm{c}} \subset \text{ any } \Omega_{\mathrm{M}} \\ 1, & \text{if } \Omega_{\mathrm{H}}^{\mathrm{c}} \not\subset \text{ any } \Omega_{\mathrm{M}} \end{cases} \tag{1}$$

where d_{cm} is the distance between the centroid of the hexagonal cell and the mask, and $\Omega_{\mathrm{H}}^{\mathrm{c}}$ represents the centroid of Ω_{H} (Fig. 1a).

Following generic topology optimization problem can be solved to get the desired continuum.

$$\begin{aligned} \underset{\mathbf{v}}{\text{minimize}} \quad & f_0(\mathbf{v}) \\ \text{subject to} \quad & g_j(\mathbf{v}) \leq 0 \end{aligned} \tag{2}$$

[3] the method is generic and can be employed to optimize any objective.

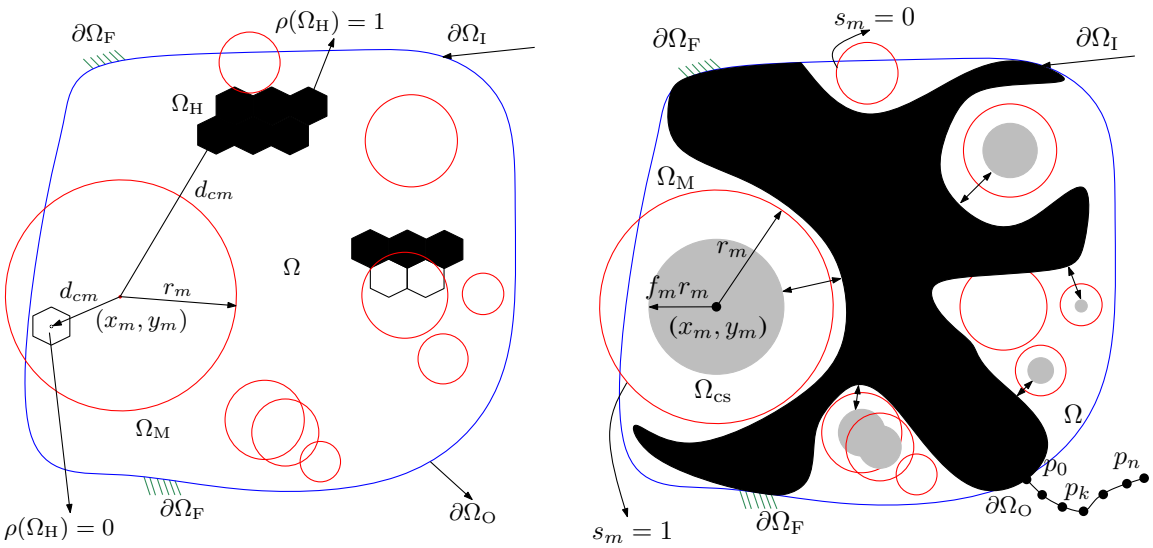

Figure 1: Hexagonal cells Ω_H are used to discretize the design domain Ω shown with superposed negative circular masks Ω_M. Masks remove the material beneath them and also, generate rigid contact surfaces. They are characterized via five parameters (x_m, y_m, r_m, s_m, and f_m). $s_m = 1$ indicates that the m^{th} mask suspends a contact surface (circular regions in grey) within it while with $s_m = 0$ the material is removed. $\rho(\Omega_H) = 0$ (cells whose centroids are inside any mask) implies that the hexagonal sub-region has no material while $\rho(\Omega_H) = 1$ (cells whose centroids are outside any mask) suggests that the cell has the desired material. Boundary(ies) of the continuum generated via $\rho(\Omega_H) = 1$ is (are) smoothened. Circular regions within masks with $s_m = 1$ interact (shown with double head arrows) with the continuum to render the desired path. Fixed boundary(ies) ($\partial\Omega_F$), input ($\partial\Omega_I$) and output ($\partial\Omega_o$) conditions are also depicted.

$f_0(\mathbf{v})$ is the desired objective and $g_j(\mathbf{v}) \leq 0$ are the imposed design constraints. $\mathbf{v}$, the design vector, comprises of a set of variables $\{(x_m, y_m, r_m)\}\ \forall\ \Omega_M$.

3.1 Contact MMOS

MMOS is extended such that masks not only remove material beneath them, but also, within some, fixed, non-deforming regions[4] are introduced to permit the continuum to physically interact with them. To accomplish this, each mask Ω_{Mi} is represented via five variables: (x_i, y_i, r_i, s_i, f_i). The first three represent the x, y coordinates of the mask center and mask radius respectively. The fourth variable s_i is discrete: $s_i = 0$ indicates absence of the contact surface Ω_{cs} within the mask while $s_i = 1$ models the presence of a circular contact region whose radius is computed as $f_i r_i, 0 \leq f_i < 1$ with its center coordinates the same as (x_i, y_i). Fig. 1b depicts the overall intent. Ideally, numerous masks individually encompassing rigid contact regions within them can convene at a site and result in a contact region of a generic shape. Realistically, however, contact regions are expected to be bounded by a set of circular arcs. In the current implementation, contact interaction is permitted only between the continuum and rigid regions introduced by the masks. It is assumed that subregions of the continuum do not interact with each other.

[4]Contact surface Ω_{CS}

4 Boundary Smoothing and Finite Element Analysis

4.1 Boundary Smoothing

Notwithstanding the efficiency in analysis, boundary smoothing [32, 33] is deemed essential to facilitate accurate large deformation contact analysis and ensure that it converges for most intermediate contact-aided compliant designs. Indirect consequences of smoothing are realizable designs (see Figs. 11 and 14) and alleviation of stress concentration regions at the boundary(ies). To ensure convergence in contact analysis, continuum boundaries (interior and exterior) should at least have slope (C^1) continuity though higher order continuity is desirable [34].

To obtain smooth boundaries, a systematic approach of boundary node shifting is used [33]. Mid-points of the outer edges of boundary cells are connected with straight line segments, and boundary nodes are projected onto these segments along their shortest perpendiculars (Fig. 2a). This smoothing step can be performed β (integer) ≥ 1 times. New positions of the boundary nodes are used in the finite element analysis, while retaining the element connectivity and positions of the interior (non-boundary) nodes. Even with the mask overlay method, increase in the number of hexagonal cells does (adversely) influence the analysis time though the smoothing process takes 5% of the total computational cost [33]. The smoothing algorithm implemented herein ensures edge-connectivity throughout [33].

In addition to removing hexagonal cells beneath the masks, regular hexagonal cells (e.g., those that are unaffected by boundary smoothing) are removed. This is equivalent to imposing a negative mask over such a cell. Such removal helps reduce the continuum volume making the latter less bulky and members slender so that they can undergo large local deformation. However, removing these cells results in new serrated boundaries. At this stage, all hexagonal cells present in the design are considered in their regular states, and boundary smoothing is performed again.

4.2 Stiffness Computation

As a result of boundary smoothing, some regular hexagonal cells get reshaped to concave ones. To cater to generic six-noded polygonal shapes, Mean-Value Co-ordinates [35, 36] based shape functions are employed. Stiffness $\mathbf{k}$ of each cell is evaluated as follows. The cell is divided into six triangular sub-regions [36, 37]. Thereafter, integration over each region is performed through a 25 Gauss-point scheme for each sub-region (Fig. 3) to ensure accuracy in computation of the stiffness of each cell. The global stiffness matrix $\mathbf{K}$ is obtained. The elemental internal force $\mathbf{r}_{\text{elem}}$ and global internal force $\mathbf{R}$ are also evaluated. Geometrically nonlinear analysis with Newton-Raphson (NR) iterations for a sequence of load increments is implemented. Within each NR iteration, contact forces between the deforming continuum and rigid bodies need to be computed which is accomplished, as in the section 5.

5 Contact Modeling and Analysis

The section describes contact modeling with geometrically and materially nonlinear deformation analysis.

Let a rigid body Ω_{cs} (contact surface: master body) come in contact with a part of the deforming body Ω_{s} (continuum: slave body) (Fig. 4). Let points P_{m} on Ω_{cs} and P_{s} on Ω_{s} have position vectors $\mathbf{x}_{\text{m}}$ and $\mathbf{x}_{\text{s}}$ respectively. Let the normal triad at P_{s} be $\mathbf{n}^{\text{s}}_a$, $a = 1, 2, 3$ and that at P_{m} be $\mathbf{n}^{\text{m}}_b$, $b = 1, 2, 3$. Consider $\mathbf{n}^c_1$, c= m, s to be outward normals and remaining to be tangential components at P_{m} and P_{s} respectively. Let the contact tractions at P_{s} and P_{m} be $\mathbf{t}_{\text{s}}$ and $\mathbf{t}_{\text{m}}$ ($\mathbf{t}_{\text{s}} = -\mathbf{t}_{\text{m}}$) respectively.

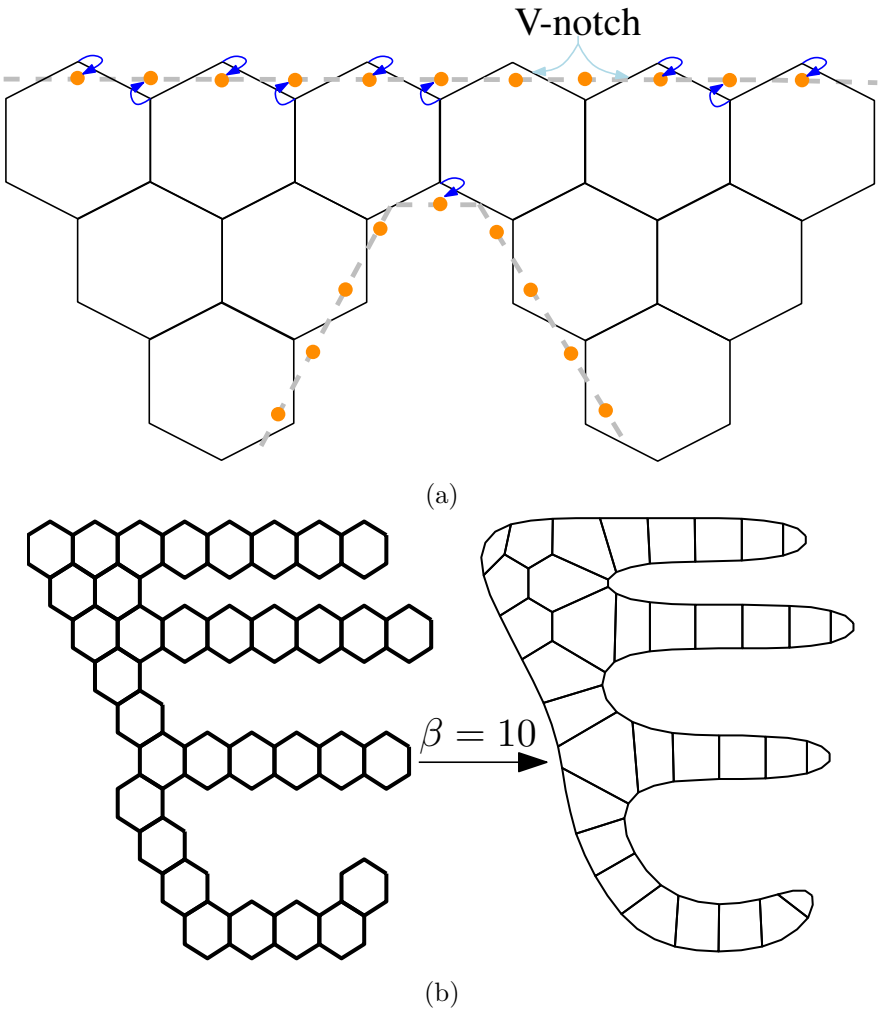

Figure 2: Boundary smoothing to facilitate contact analysis. (a) Mid-points of boundary edges are joined with straight lines and boundary nodes shifted along their shortest perpendicular distances on these segments. (b) Boundary smoothing with $\beta = 10$ steps.

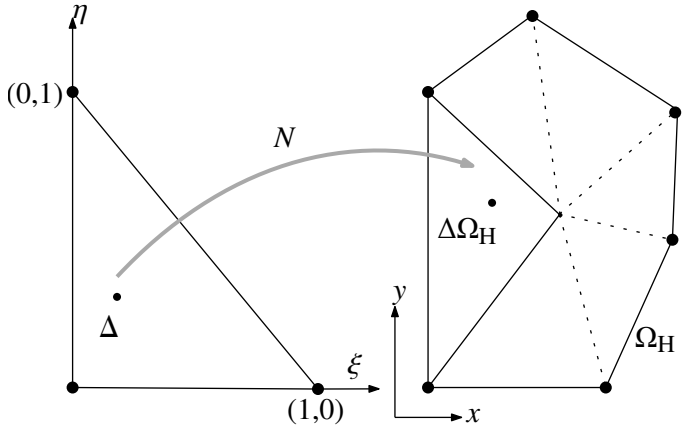

Figure 3: Each cell is divided into six subregions and integration over each subregion is performed to evaluate the element stiffness matrix **k**.

A point P_s on the slave surface is taken. Its distance from all points on the master surface(s) is computed. P_m is found such that it is most proximal to P_s. This procedure is followed for

all points on Ω_s.

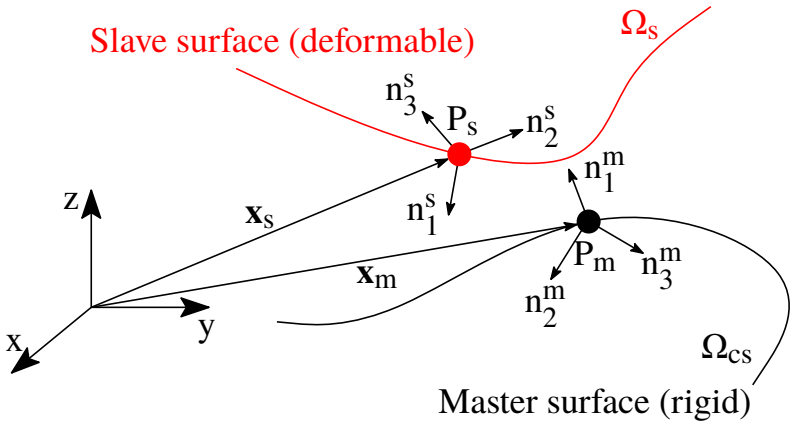

Figure 4: Contact formulation of the two bodies Ω_s and Ω_{cs} in their current configuration. Normal triad on P_s are n_i^s and that on P_m are n_i^m, where $i = 1, 2, 3$.

The gap $\mathbf{g}$ is computed as

$$\mathbf{g} = \mathbf{x}_s - \mathbf{x}_m \tag{3}$$

The normal gap g_n can be defined via either $(\mathbf{x}_s - \mathbf{x}_m).\mathbf{n}_1^m$ or $(\mathbf{x}_m - \mathbf{x}_s).\mathbf{n}_1^s$. When $g_n < 0$, contact is detected. The following impenetrability condition is then imposed.

$$\begin{aligned} (\mathbf{x}_s - \mathbf{x}_m).\mathbf{n}_1^m &= 0 \\ (\mathbf{x}_m - \mathbf{x}_s).\mathbf{n}_1^s &= 0 \end{aligned} \tag{4}$$

When the surfaces are in contact or intersecting, traction components along the outward normals $\mathbf{n}_1^c$ are compressive (< 0), otherwise they are zero.

$$t_1^c = \mathbf{t}^c.\mathbf{n}_1^c \leq 0; \qquad c = \mathrm{m}, \mathrm{s} \tag{5}$$

To check for slipping/sliding

$$t_2^c = \mathbf{t}^c.\mathbf{n}_2^c \text{ and } t_3^c = \mathbf{t}^c.\mathbf{n}_3^c; \qquad c = \mathrm{m}, \mathrm{s} \tag{6}$$

are used. $(t_2^c \cdot t_2^c + t_3^c \cdot t_3^c)^{\frac{1}{2}} < \mu(t_1^c)$ for stiction, else for sliding, equality sign is used. Newton-Raphson iterations guide g_n to become zero so that impenetrability conditions are satisfied and traction forces computed. Implementation details are provided in Reference [38]. To model contact problems herein, impact is assumed absent. In addition to contact conditions, relations for equilibrium, strain displacement, constitutive and boundary restraints can be written mathematically as

$$\begin{aligned} \sigma_{ij,j}(\mathbf{x}) + b_i(\mathbf{x}) &= 0,\ \mathbf{x} \in \Omega_{cs}, \Omega_s \\ \epsilon_{ij}(\mathbf{x}) &= 0.5(u_{i,j} + u_{j,i} + u_{i,k}u_{k,j}) \\ S_{ij}(\mathbf{x}) &= E_{ijkl}\epsilon_{kl}(\mathbf{x}) \\ \mathbf{u}(\Gamma_{dc}) &= \mathbf{u}_c,\ c = m, s \\ \sigma_{ij}(\Gamma_{Fc})n_j(\Gamma_{Fc}) &= f_i(\Gamma_{Fc}) \end{aligned} \tag{7}$$

σ_{ij} and ϵ_{ij} represent the Cauchy stress and Green-Lagrange strain tensor components respectively. b_i is the body force, S_{ij} is the second Piola-Kirchoff stress tensor, E_{ijkl} is the elastic tensor (we employ the neo-Hookean plane strain material model), Γ_{dc} represent boundaries on two surfaces, where displacements $\boldsymbol{u}_c$ is known a priori, and tractions f_i are imposed on surfaces Γ_{Fc} of the two bodies. The transformation, $\mathbf{S} = \det(\mathbf{F})\mathbf{F}^{-1}.\boldsymbol{\sigma}.\mathbf{F}^{-\mathrm{T}}$ is employed to relate Cauchy stress and second Piola-Kirchoff stress tensors.

5.1 Multiple Contact

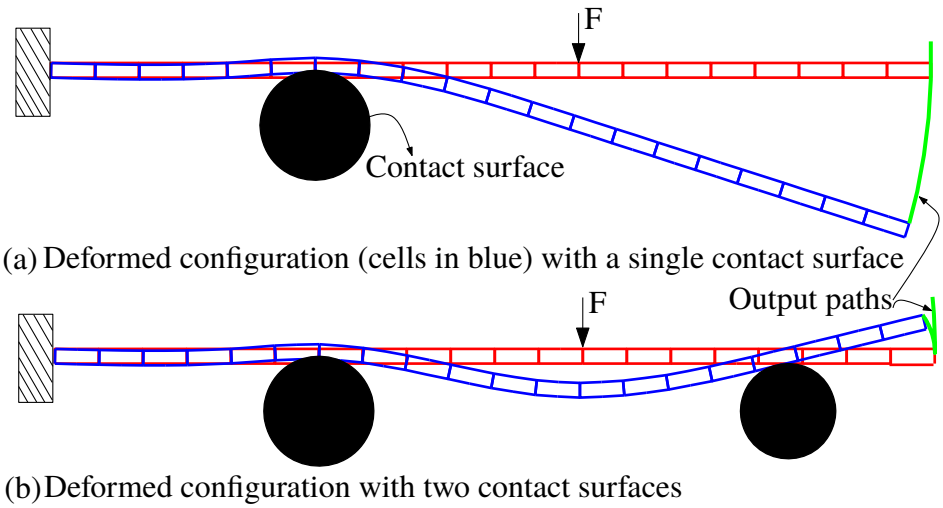

(a) Deformed configuration (cells in blue) with a single contact surface

(b) Deformed configuration with two contact surfaces

Figure 5: Example of single and multiple contact analysis with a cantiliver beam. Depending on nature of contact, back tracking (a) of the output port (the beam tip) or a kink (b) is observed.

Many contact surfaces get generated during evolution of a CCM. Depending on their positions, shapes and sizes, these contact surfaces may either interact with the continuum or lay passive. Interaction of the continuum with multiple contact surfaces cannot be ruled out. The proposed topology optimization algorithm during synthesis, automatically determines shapes and sizes of flexible members in a deforming continuum, and rigid (target) surfaces with which the continuum is deemed to come into contact (see section 3). The formulation and numerical implementation of the nonlinear finite element analysis with contact briefed in sections 4 and 5, and detailed in Reference [38] accurately determines the members coming into contact and the associated contact forces. The code for 2D contact analysis developed inhouse, caters to all surface geometries and possibilities, e.g., point and/or line, and single/multiple contacts. Fig. 5 exhibits certain cases.

6 Problem Formulation

6.1 Fourier Shape Descriptors

Fourier Shape Descriptors (FSDs) [25] are employed to evaluate discrepancies between the obtained and prescribed paths. Objective based on FSDs allows a user to control errors in the shape, size, and orientation between the actual and desired paths, independently. Previously, FSDs based objective is employed successfully in References [24, 26, 28, 30] to achieve the path generating mechanisms. A brief discussion on FSDs is given below.

Let the output path be represented discretely via its vertices $\mathrm{P}_0, \mathrm{P}_1, \cdots, \mathrm{P}_\mathrm{M}$ in a clockwise sense, wherein $\mathrm{P}_0 \equiv \mathrm{P}_\mathrm{M}$ (Fig. 6). Length of the i^{th} segment between vertices P_{i-1} and P_i is ΔL_i. The initial orientation of the desired path is θ_δ. L_δ represents the total length of the prescribed curve. The Curve is modeled by a normalized periodic function $\phi^*(t) = \phi(\frac{L_\delta t}{2\pi}) + t$, wherein t is a parameter and defined by $\frac{2\pi l_k}{L_\delta}$, $t \in [0, 2\pi]$. Since $\phi^*(0) = \phi^*(2\pi) = 0$, $\phi^*(t)$ can be expressed via a Fourier series as:

$$\phi^*(t) = a_0 + \sum_{k=1}^{\infty} \{a_k \cos kt + b_k \sin kt\} \tag{8}$$

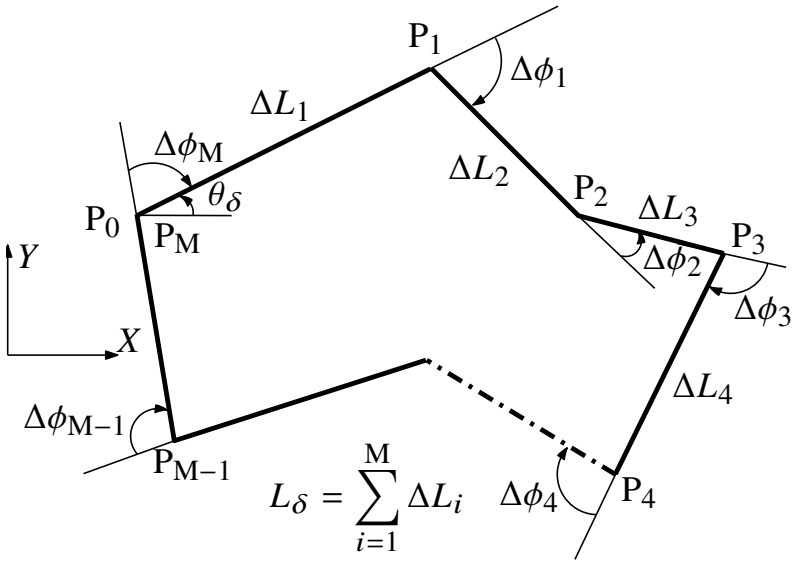

Figure 6: Evaluation of Fourier Shape Descriptors

where a_0, $a_k$and b_k are Fourier coefficients evaluated as follows:

$$\begin{aligned} a_0 &= \frac{1}{2\pi}\int_0^{2\pi} \phi^*(t)dt \\ a_n &= \frac{1}{\pi}\int_0^{2\pi} \phi^*(t)\sin dt \approx -\frac{1}{n\pi}\sum_{k=1}^{N}\Delta\phi_k \cos\left(\frac{2\pi n l_k}{L_\delta}\right) \\ b_n &= \frac{1}{\pi}\int_0^{2\pi} \phi^*(t)\cos ntdt \approx -\frac{1}{n\pi}\sum_{k=1}^{N}\Delta\phi_k \sin\left(\frac{2\pi n l_k}{L_\delta}\right) \end{aligned} \tag{9}$$

wherein, $l_k = \sum_{i=1}^{k}\Delta L_i$

Let the Fourier coefficients of the actual path traced by a candidate design be a_α and b_α and that of the desired path be a_δ and b_δ. Let the length of the desired path be L_δ and that of the actual path be L_α. Let the initial orientations with the horizontal, of the two paths be given by θ_δ and θ_α respectively. The objective is constructed as the weighted sum of the errors in each coefficient, length and orientation, as below.

$$f_0(\mathbf{v}) = \lambda_a a_{\text{err}} + \lambda_b b_{\text{err}} + \lambda_L L_{\text{err}} + \lambda_\theta \theta_{\text{err}} \tag{10}$$

where λ_a, λ_b, λ_L, and λ_θ are user defined weights. These errors are evaluated as

$$\begin{aligned} a_{\text{err}} &= \sum_{f=1}^{N}(a_\delta - a_\alpha)^2; \qquad b_{\text{err}} = \sum_{f=1}^{N}(b_\delta - b_\alpha)^2 \\ L_{\text{err}} &= (L_\delta - L_\alpha)^2; \qquad \theta_{\text{err}} = (\theta_\delta - \theta_\alpha)^2 \end{aligned} \tag{11}$$

6.2 Resource Constraint

The term, $\{V_{\text{err}} = (V^c - V^*)\}$ is introduced in the objective (Eq. 10), where V^c and V^* are the current and permitted volumes of the continuum respectively. The modified objective is:

$$f_0^m(\mathbf{v}) = f_0(\mathbf{v}) + \lambda_v V_{\text{err}} \tag{12}$$

where λ_v, the resource penalty parameter, is used to steer the search algorithm towards a desired CCM with permitted resource volume. If $V^c - V^* > 0$, λ_v is positive, else, it is zero.

6.3 Search Algorithm

To minimize the objective, we employ a random mutation based stochastic, hill climber search. An initial solution $\mathbf{v}_0$ is taken and made to undergo several mutations to sequentially improve the objective. Maximum number of iterations $\mathrm{I}_{\mathrm{mmos}}$ is fixed a priori. For N_{m} masks, the total number of variables in $\mathbf{v}_0$ are $5N_{\mathrm{m}}$. Let the probability to mutate a variable $d \in \mathbf{v}_0$ be pr, (chosen 0.08 herein). In an iteration, a random number ζ is generated for each variable. If $\zeta < pr$, the corresponding variable is modified as $d_{\mathrm{n}} = d \pm (c \times m_{\max})$ where c is a random number and $m_{\max}$ is used as 25% of the domain size. Variables x_i, y_i, r_i, f_i and s_i of a mask are mutated as above. As s_i is binary, an additional check is performed. If $s_i < 0.5$, $s_i = 0$ is imposed, else, $s_i = 1$ is taken. The aforementioned mutations lead to a new design $\mathbf{v}_n$ which is evaluated using the finite element analysis and Fourier Shape Descriptors. If found better, $\mathbf{v}_0$ is replaced by $\mathbf{v}_n$. The search process is continued until $\mathrm{I}_{\mathrm{mmos}}$ iterations are reached. The search algorithm is shown in Fig. 7. Cardinal reasons to employ stochastic search are: (a) Cell densities should either be 0 or 1 for otherwise ambiguity in interpreting the continuum may lead to incomplete/poor realization of the solution, and (b) non-convergence during Newton-Raphson iterations in the finite element analysis can stall a gradient search process as the latter is based on point-to-point evaluation. For subsequent advancement to the next step of search, convergence in analysis in the previous step is necessary. For any intermediate continuum, accomplishment of geometrically nonlinear analysis, and with contact in particular, cannot be guaranteed.

7 Synthesis Examples

Below, using the same initial design region and input and output ports, generic path generating examples, with different paths having one kink each, are solved to showcase the efficacy and versatility of the proposed synthesis method for contact-aided compliant mechanisms.

7.1 Example 1

Figure 8 depicts the design specifications and Table 1 includes details on the various parameters used to generate the designs: The design region is represented using 25 hexagonal cells each along the horizontal and vertical directions. Each cell is inscribed within a circle of unit radius. 10 masks along the horizontal and 8 along the vertical are taken. Minimum and maximum mask radii are taken as 0.1 mm and 6 mm respectively. Out of plane thickness is 5 mm, Elastic modulus is 2100 MPa, and Poisson's ratio is 0.30. For the hill climber search, probability that a variable can mutate is taken as 0.08. Maximum number of search iterations I_{mmos} are set to 40,000. Input load is also considered a design variable whose lower and upper bounds are set to -2000 N and 2000 N. Note that direction of the input load is permitted to change. Maximum radius achievable for the contact surface is 3 mm (i.e., $f_i(\max) = 0.5$). Number of boundary smoothing steps performed for each candidate continuum is 10. Among other parameters, weights of the Fourier Shape Descriptors are set to $\lambda_{\mathrm{a}} = 30$ and $\lambda_{\mathrm{b}} = 30$. Weight for discrepancy in the length is taken as $\lambda_{\mathrm{L}} = 1$ while that for the orientation is $\lambda_\theta = 0.1$. V^* is taken as 30% of the maximum possible volume V. λ_v is taken as 15 if the continuum volume V^c exceeds V^*, else, λ_v is set to 0. Fig. 9 shows the undeformed optimized continuum and the final deformed continuum with all solid contact surfaces. The final obtained input force in the horizontal direction is 105.27 N. The CCM is obtained after 6513 search iterations. Intermediate deformed configurations with only active contact region, and comparison of paths are depicted

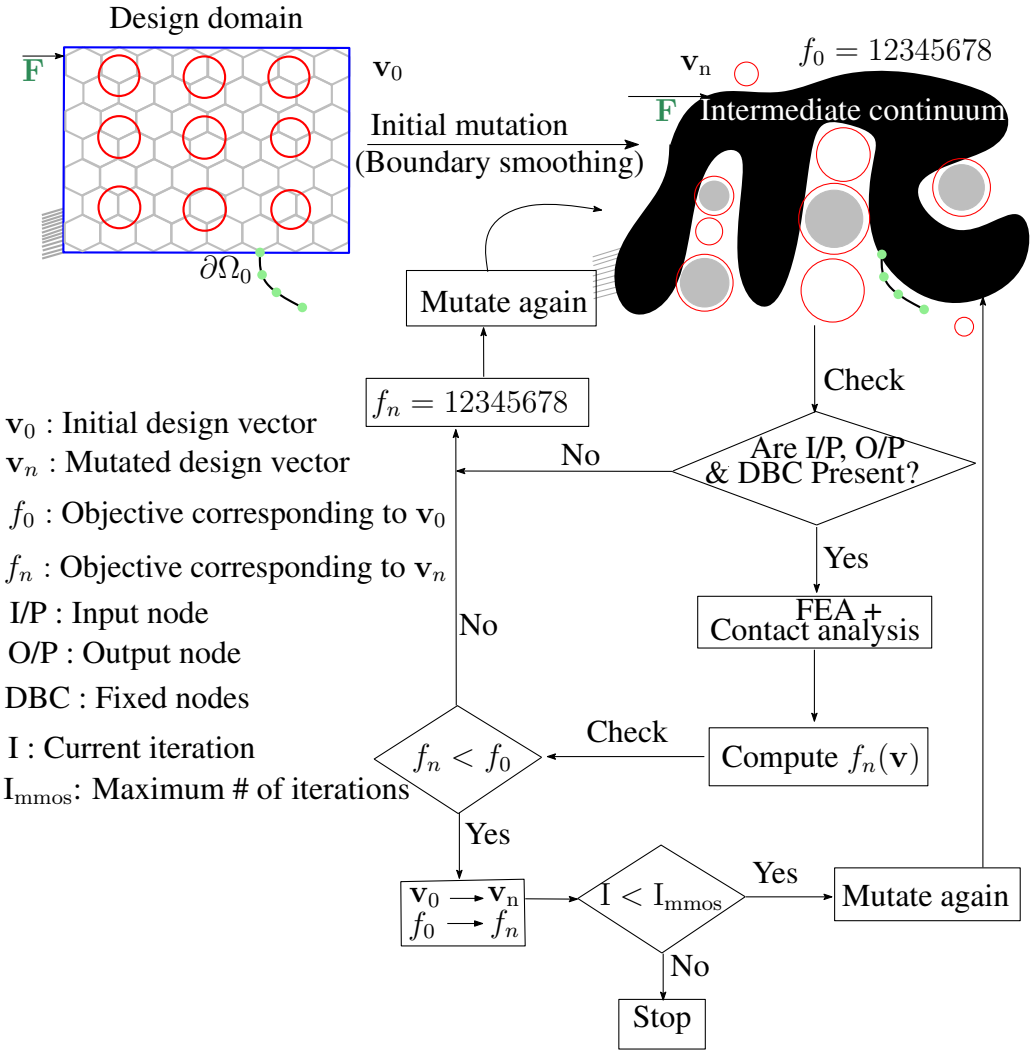

Figure 7: Ω is discretized via hexagonal cells Ω_{H}. Negative circular masks Ω_{M} are employed to remove the material and to encompass contact surfaces within some. Contact analysis with minimization of Fourier Shape Descriptors based objective is performed to achieve the path close to that desired.

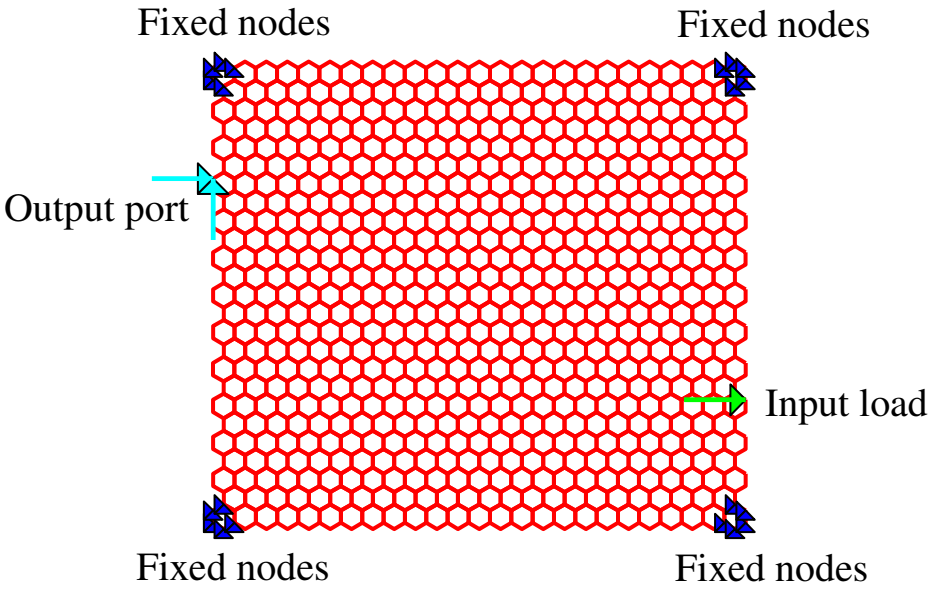

Figure 8: Design specifications for the synthesis of CCMs

.

in Fig. 10. Fig. 11 shows the fabricated continuum in its intermediate deformed configurations. The path shapes in Figs. 10(d) and 11(d) compare well.

Table 1: Parameters used in the synthesis. Herein, HCH represents the number of hexagonal cells in the horizontal direction and HCV indicates the number of hexagonal cells in the vertical direction.

Parameter's name	**Value**
Design domain (HCH × HCV)	25×25
Number of Ω_{M} in x-direction ($\mathrm{N_x}$)	10
Number of Ω_{M} in y-direction ($\mathrm{N_y}$)	8
Maximum radius of Ω_{M}	6.0 mm
Minimum radius of Ω_{M}	0.1 mm
Maximum number of iterations	40000
Out of plane thickness	5.0 mm
Young's modulus	2100 MPa
Poisson's ratio	0.30
Permitted volume fraction ($\frac{V^*}{V}$)	0.30
Mutation probability	0.08
Contact surface radii factor	0.50
Maximum mutation size ($m_{\max}$)	6
Upper limit for input load	2000 N
Lower limit for input load	-2000 N
Weight for a_{err} (λ_{a})	30
Weight for b_{err} (λ_{b})	30
Weight for path length error (λ_{L})	1
Weight for path orientation error (λ_θ)	0.1
Boundary smoothing steps (β)	10

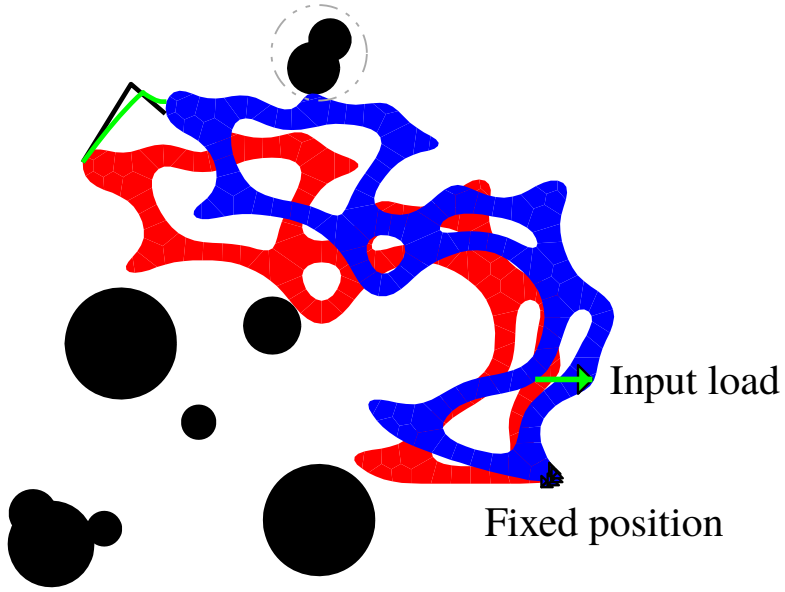

Figure 9: Undeformed (red solid), deformed (blue solid), contact surfaces (black solid), the desired path (black curve) and the actual path (green curve) are shown. Active contact surfaces are enclosed within dash-dotted circle.

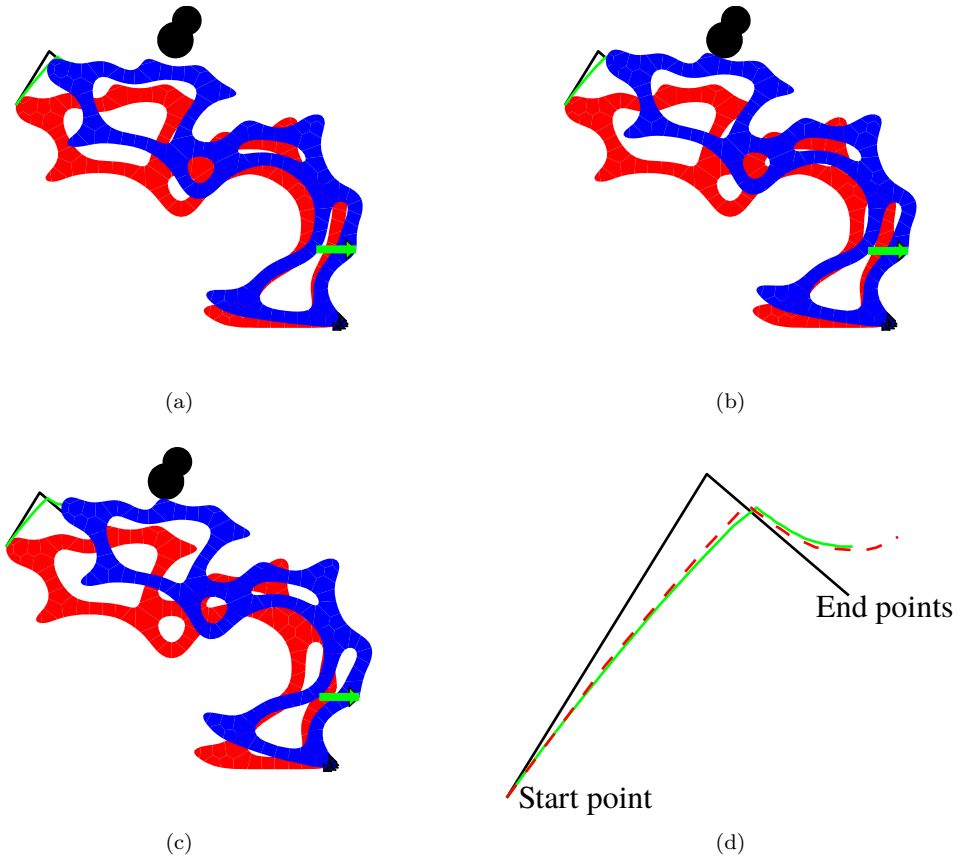

(a) (b) (c) (d)

Figure 10: Different deformed configurations are shown in (a), (b) and (c). (d) compares the desired path (black), the actual path (green) and that using Abaqus (red dotted) with neo-Hookean material and 4 noded plain strain (CPE4I) elements.

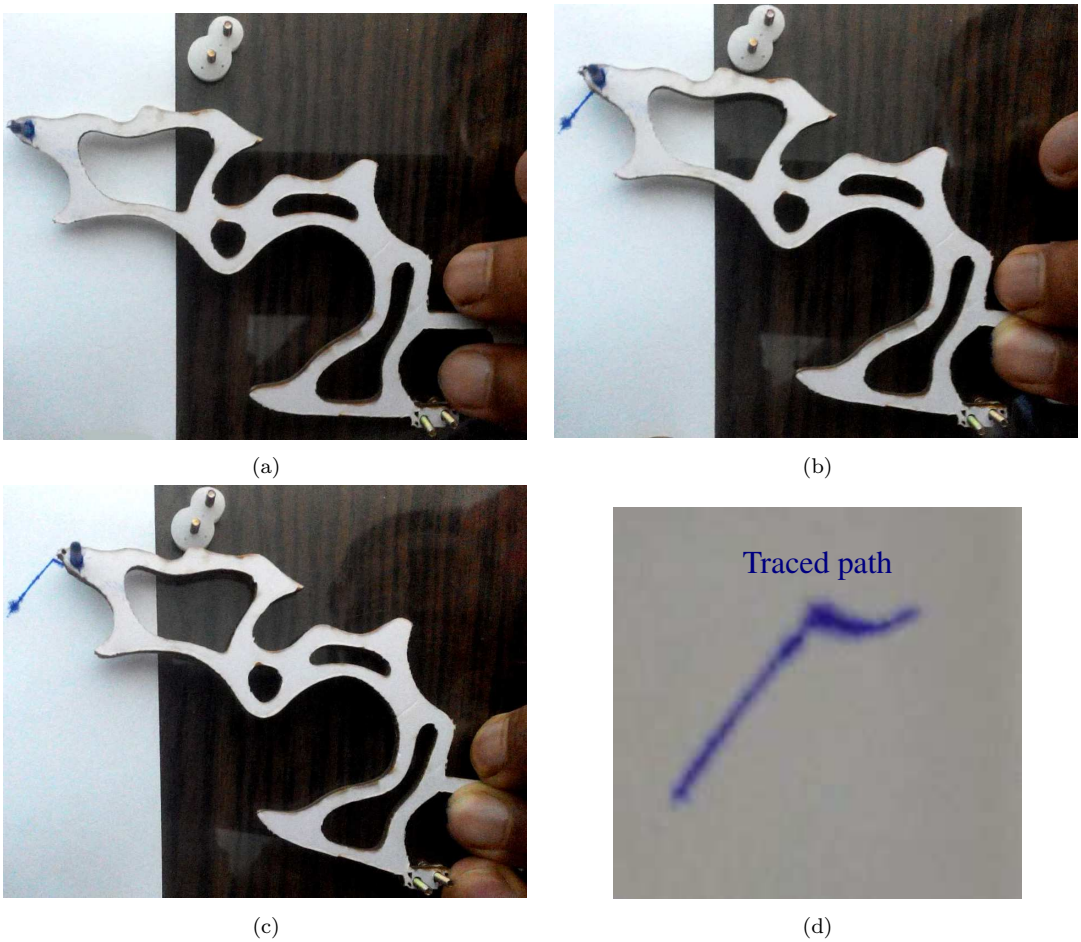

(a) (b) (c) (d)

Figure 11: Different deformed configurations of the fabricated prototype for Example 1 are shown in (a), (b), and (c). (d) shows the traced path.

7.2 Example 2

Design specifications and values of various parameters used in this example are identical to those in Example 1. However, the prescribed path is different. Fig. 12 shows the undeformed optimized continuum and the final deformed continuum with all solid contact surfaces. The final obtained input force along the positive horizontal direction is 106.45 N. The CCM is obtained after 5971 search iterations. Fig. 13 depicts intermediate configurations with only one active contact surface and compares the desired and obtained paths. Intermediate deformed configurations of the fabricated prototype are depicted in Fig. 14 suggesting close resemblance in the path shapes (Figs. 13d and 14d).

8 Discussion and Conclusion

In previous works on topology synthesis of CCMs, design [28, 29] representation used is with initially straight frame elements and contact surfaces are prescribed. In Reference [30], initially curved frame elements are employed and contact surfaces identified systematically using a commercial software. Herein, we present a continuum based topology optimization approach to synthesize such mechanisms via the modified Material Mask Overlay Method (CMMOS). Hexagonal cells are used to discretize the design space. Negative masks are employed not only to remove material, but also, to generate rigid contact surfaces within some of them. Boundary

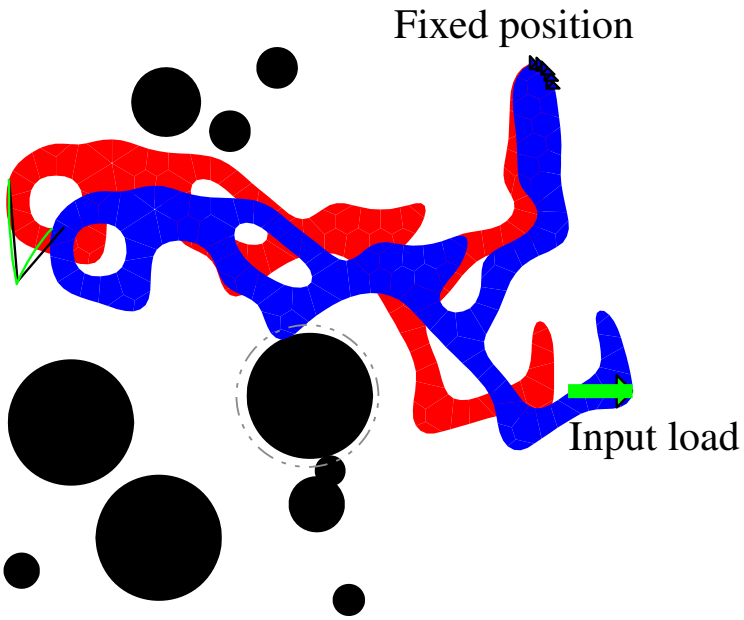

Figure 12: Undeformed (red solid), deformed (blue solid), contact surfaces (black solid), the desired path (black curve) and the actual path (green curve) are shown. Active contact surfaces are enclosed within dash-dotted circle.

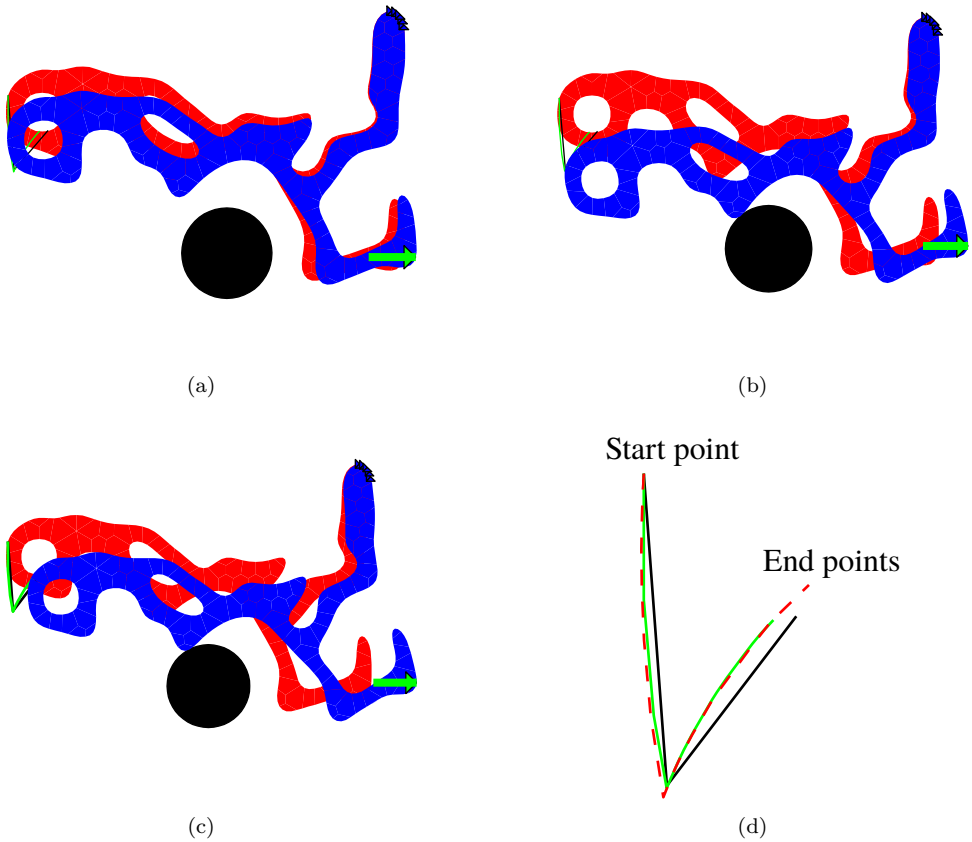

Figure 13: Different deformed configurations are shown in (a), (b) and (c). (d) shows comparison of the desired path (black), the actual path (green) and that using Abaqus (red dotted) with neo-Hookean material and 4 noded plane strain (CPE4I) elements.

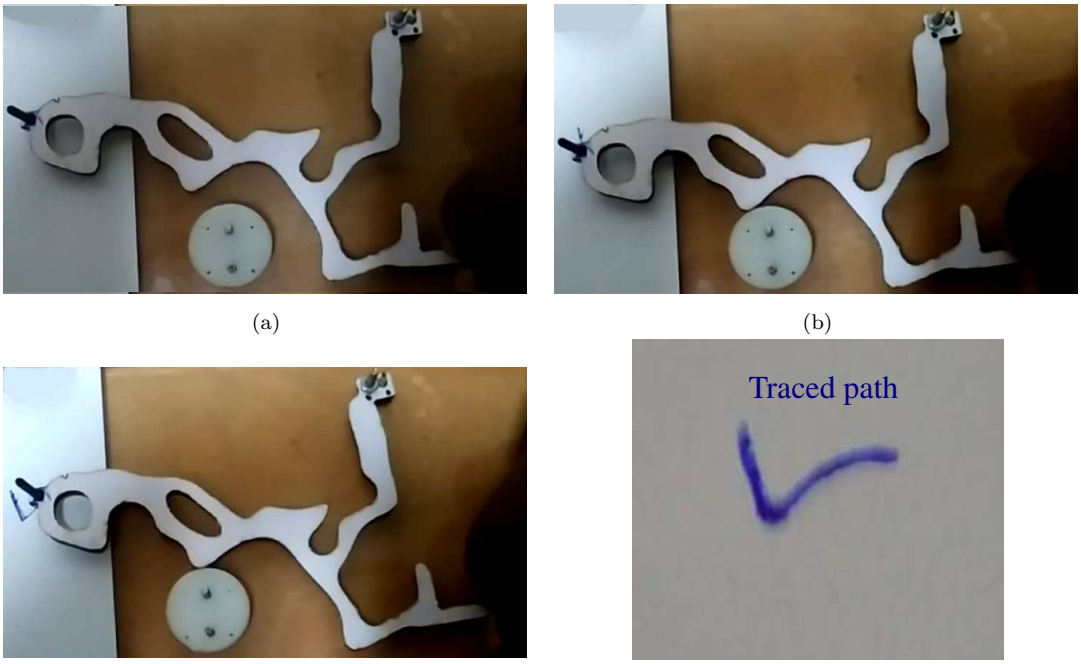

(a) (b) (c) (d)

Figure 14: Different deformed configurations of the fabricated prototype for Example 2 are shown in (a), (b), and (c). (d) shows the traced path.

smoothing is implemented to facilitate contact analysis. Mean-Value Coordinates based shape functions are used to cater to generic six-noded polygonal cells. A stochastic hill climber search is implemented to minimize the Fourier Shape Descriptors based objective to obtain the desired non-smooth path. The search also helps determine the interacting surfaces systematically. Preliminary results are promising and the methodology is generic in that the proposed continuum optimization method can be employed to synthesize, not only path generating contact-aided compliant mechanisms, but also, those with, say static balancing and negative stiffness characteristics.

Two examples are presented with the same design specifications but for non-smooth desired paths of different shapes and sizes with kinks at different locations. The synthesized examples and their deformed histories (Figs. 9, 10, 12, and 13), and behavior of the respective prototypes (Figs. 11 and 14) suggest that the obtained paths are 'optimally proximal' in shape and size to those respectively prescribed. In both cases, presence of kinks (sharp corners in the output paths) correspond to occurrence of contact between the deforming continuum and the neighboring rigid surface(s). As observed in the examples, the output path can be obtained quite accurately if the input port is guided suitably along the prescribed direction. Better solutions are possible if the synthesis process is not restricted by the specified design constraints and limited (specified) computational effort. The algorithm suggests numerous contact surfaces (Figs. 9 and 12), but only some participate actively in contact. Comparing with the partially compliant solutions (Figs. 5 g-h) in Reference [27] synthesized using similar specifications, one observes that a single instance of contact between the deforming continuum and the rigid body in the neighborhood (Fig. 9) seems adequate to generate a desired kink on the output path as opposed to a number of revolute joints. It has also been established therein via the synthesis of partially compliant and fully complaint mechanisms for C^0 continuous paths, that a kink in the output path of a singlepiece continuum cannot be observed unless there is a geometric/material cause for the continuum to suddenly alter its deformation characteristics.

The final CCMs are also analyzed in Abaqus with neo-Hookean material and 4 noded plain-

strain elements (CPE4I) using the respective optimal forces, boundary conditions and active contact surfaces. Analyses suggest that the obtained paths closely follow those respective paths traced by CCMs (Figs. 10d and 13d).

As search is stochastic (computational expenses is expected to be high), it may not quickly lead to first meaningful[5] intermediate configuration. Such cases should be ceased and reinitiated because, they may increase the computational cost significantly.

Though self contact lies outside the scope of the work presented herein, its implementation and related examples with both self and mutual contact will be presented in future.

References

[1] M. P. Bendsøe and N. Kikuchi, "Generating optimal topologies in structural design using a homogenization method," *Computer methods in applied mechanics and engineering*, vol. 71, no. 2, pp. 197–224, 1988.

[2] G. Ananthasuresh, S. Kota, and Y. Gianchandani, "A methodical approach to the design of compliant micromechanisms," in *Solid-state sensor and actuator workshop*, vol. 1994, pp. 189–192, SC: IEEE, 1994.

[3] G. Ananthasuresh, S. Kota, and N. Kikuchi, "Strategies for systematic synthesis of compliant mems," in *Proceedings of the 1994 ASME winter annual meeting*, pp. 677–686, 1994.

[4] M. Frecker, G. Ananthasuresh, S. Nishiwaki, N. Kikuchi, and S. Kota, "Topological synthesis of compliant mechanisms using multi-criteria optimization," *Journal of Mechanical design*, vol. 119, no. 2, pp. 238–245, 1997.

[5] S. Nishiwaki, M. I. Frecker, S. Min, and N. Kikuchi, "Topology optimization of compliant mechanisms using the homogenization method," 1998.

[6] G. Rozvany, M. Zhou, and T. Birker, "Generalized shape optimization without homogenization," *Structural Optimization*, vol. 4, no. 3-4, pp. 250–252, 1992.

[7] M. P. Bendsøe, "Optimal shape design as a material distribution problem," *Structural optimization*, vol. 1, no. 4, pp. 193–202, 1989.

[8] M. Bendsoe, "Methods for optimization of structural topology, shape and material," 1995.

[9] O. Sigmund, "On the design of compliant mechanisms using topology optimization*," *Journal of Structural Mechanics*, vol. 25, no. 4, pp. 493–524, 1997.

[10] L. Yin and G. Ananthasuresh, "Topology optimization of compliant mechanisms with multiple materials using a peak function material interpolation scheme," *Structural and Multidisciplinary Optimization*, vol. 23, no. 1, pp. 49–62, 2001.

[11] R. Saxena and A. Saxena, "On honeycomb representation and sigmoid material assignment in optimal topology synthesis of compliant mechanisms," *Finite Elements in Analysis and Design*, vol. 43, no. 14, pp. 1082–1098, 2007.

[12] S. Rahmatalla and C. C. Swan, "Sparse monolithic compliant mechanisms using continuum structural topology optimization," *International Journal for Numerical Methods in Engineering*, vol. 62, no. 12, pp. 1579–1605, 2005.

[5] a solution with NR iterations converging, with or without contact

[13] J. K. Guest, J. Prévost, and T. Belytschko, "Achieving minimum length scale in topology optimization using nodal design variables and projection functions," *International Journal for Numerical Methods in Engineering*, vol. 61, no. 2, pp. 238–254, 2004.

[14] M. Y. Wang, X. Wang, and D. Guo, "A level set method for structural topology optimization," *Computer methods in applied mechanics and engineering*, vol. 192, no. 1, pp. 227–246, 2003.

[15] M. Y. Wang, S. Chen, X. Wang, and Y. Mei, "Design of multimaterial compliant mechanisms using level-set methods," *Journal of Mechanical Design*, vol. 127, p. 941, 2005.

[16] M. Langelaar, "The use of convex uniform honeycomb tessellations in structural topology optimization," in *7th world congress on structural and multidisciplinary optimization, Seoul, South Korea, May*, pp. 21–25, 2007.

[17] C. Talischi, G. H. Paulino, and C. H. Le, "Honeycomb wachspress finite elements for structural topology optimization," *Structural and Multidisciplinary Optimization*, vol. 37, no. 6, pp. 569–583, 2009.

[18] A. Saxena, "Topology design with negative masks using gradient search," *Structural and Multidisciplinary Optimization*, vol. 44, no. 5, pp. 629–649, 2011.

[19] A. Saxena, R. Sauer, *et al.*, "Combined gradient-stochastic optimization with negative circular masks for large deformation topologies," *International Journal for Numerical Methods in Engineering*, vol. 93, no. 6, pp. 635–663, 2012.

[20] A. Saxena and G. Ananthasuresh, "On an optimal property of compliant topologies," *Structural and multidisciplinary optimization*, vol. 19, no. 1, pp. 36–49, 2000.

[21] A. Saxena and G. Ananthasuresh, "Topology synthesis of compliant mechanisms for nonlinear force-deflection and curved path specifications," *Journal of Mechanical Design*, vol. 123, no. 1, pp. 33–42, 2001.

[22] C. B. Pedersen, T. Buhl, and O. Sigmund, "Topology synthesis of large-displacement compliant mechanisms," *International Journal for numerical methods in engineering*, vol. 50, no. 12, pp. 2683–2705, 2001.

[23] A. Saxena, "Synthesis of compliant mechanisms for path generation using genetic algorithm," *Journal of Mechanical Design*, vol. 127, no. 4, pp. 745–752, 2005.

[24] I. Ullah and S. Kota, "Optimal synthesis of mechanisms for path generation using fourier descriptors and global search methods," *Journal of Mechanical Design*, vol. 119, no. 4, pp. 504–510, 1997.

[25] C. T. Zahn and R. Z. Roskies, "Fourier descriptors for plane closed curves," *Computers, IEEE Transactions on*, vol. 100, no. 3, pp. 269–281, 1972.

[26] A. K. Rai, A. Saxena, and N. D. Mankame, "Synthesis of path generating compliant mechanisms using initially curved frame elements," *Journal of Mechanical Design*, vol. 129, no. 10, pp. 1056–1063, 2007.

[27] A. K. Rai, A. Saxena, and N. D. Mankame, "Unified synthesis of compact planar path-generating linkages with rigid and deformable members," *Structural and Multidisciplinary Optimization*, vol. 41, no. 6, pp. 863–879, 2010.

[28] N. D. Mankame and G. Ananthasuresh, "Topology optimization for synthesis of contact-aided compliant mechanisms using regularized contact modeling," *Computers & structures*, vol. 82, no. 15, pp. 1267–1290, 2004.

[29] N. Mankame and G. Ananthasuresh, "Synthesis of contact-aided compliant mechanisms for non-smooth path generation," *International Journal for Numerical Methods in Engineering*, vol. 69, no. 12, pp. 2564–2605, 2007.

[30] B. N. Reddy, S. V. Naik, and A. Saxena, "Systematic synthesis of large displacement contact-aided monolithic compliant mechanisms," *Journal of Mechanical Design*, vol. 134, no. 1, p. 011007, 2012.

[31] A. Saxena, "A material-mask overlay strategy for continuum topology optimization of compliant mechanisms using honeycomb discretization," *Journal of Mechanical Design*, vol. 130, p. 082304, 2008.

[32] P. Kumar and A. Saxena, "On embedded recursive boundary smoothing in topology optimization with polygonal mesh and negative masks," *AMM india, IIT Roorkee*, pp. 568–575, 2013.

[33] P. Kumar and A. Saxena, "On topology optimization with embedded boundary resolution and smoothing," *Structural and Multidisciplinary Optimization*, vol. 52, no. 6, pp. 1135–1159, 2015.

[34] C. J. Corbett and R. A. Sauer, "Nurbs-enriched contact finite elements," *Computer Methods in Applied Mechanics and Engineering*, vol. 275, pp. 55–75, 2014.

[35] M. S. Floater, "Mean value coordinates," *Computer Aided Geometric Design*, vol. 20, no. 1, pp. 19–27, 2003.

[36] N. Sukumar and E. Malsch, "Recent advances in the construction of polygonal finite element interpolants," *Archives of Computational Methods in Engineering*, vol. 13, no. 1, pp. 129–163, 2006.

[37] N. Sukumar and A. Tabarraei, "Conforming polygonal finite elements," *International Journal for Numerical Methods in Engineering*, vol. 61, no. 12, pp. 2045–2066, 2004.

[38] P. Wriggers, *Computational contact mechanics*, vol. 30167. Springer.